



Self-similarity Characteristics of Vertical Axis Wind Turbine Wakes

X. Y. Zhang^{1†}, D. Li¹, H. J. Yan¹, Z. Li¹, Y. H. Li² and X. B. Zhang³

¹ School of New Energy and Power Engineering, Lanzhou Jiaotong University, Lanzhou 730070, China

² State Power Investment Corporation Beijing Electric Power Co., Ltd., Beijing 100029, China

³ Lanzhou Railway Bureau Jiayuguan Vehicle Section, Jiayuguan 735100, China

†Corresponding Author Email: xyzhang@lztu.edu.cn

(Received October 21, 2021; accepted March 29, 2022)

ABSTRACT

Wake generated by wind turbine can greatly influence the performance of downstream turbine. To better understand the wake self-similarity characteristics of vertical axis wind turbine (VAWT), the shear stress transport (SST) turbulence model with the addition of the γ - Re_{θ} transition model is performed to model a two-blade VAWT at different operating conditions. The simulated blade surface pressure and torque are compared with existing experimental results for validation. Results show that, the simulated results after considering the transition model are more consistent with the experimental results. Analysis of the flow field shows that the average streamwise velocity of the wake in the horizontal plane under different tip speed ratios is asymmetry, but symmetric in the vertical plane. Further analysis indicates that, at different downstream positions, the non-dimensional streamwise velocity deficit in the vertical plane remains self-similarity and basically coincides with the Gaussian distribution curve exclude the wake edges. In addition, the larger the tip speed ratio, the easier streamwise velocity deficit reach self-similarity state at downstream of the VAWT. The results of this study will be helpful to establish the wake model of the VAWT.

Keywords: Vertical axis wind turbine; Wake; Self-similarity; CFD; Tip speed ratio.

NOMENCLATURE

c	chord length	U_{∞}	inflow wind speed
C_p	pressure coefficient	U_j	velocity component
D	diameter of the wind turbine rotor	U_w	wind speed at the wake region
$E_{\gamma 1}; E_{\gamma 2}$	transition source	\mathbf{v}	velocity vector
\mathbf{f}	body force vector per unit mass	x	chordwise position
$f(\xi)$	non-dimensional shape function	γ	intermittent factor
F_{length}	length function	δU	streamwise velocity deficit
$F_{\text{onset}}; F_{\text{turb}}$	transition control function	δU_{max}	maximum streamwise velocity deficit
$r(z)$	radial distance	θ	azimuth angle
$r_{1/2}(z)$	half width of the wake	λ	tip speed ratio
p	pressure	μ	molecular viscosity
P	pressure of the blade surface	μ_t	eddy viscosity
$P_{\gamma 1}; P_{\gamma 2}$	transition source	ξ	independent variable of the shape function
R	radius of the wind turbine rotor	ρ	air density
Re_{θ}	momentum-thickness Reynolds number	$\boldsymbol{\tau}$	surface stress vector
S	strain rate	ω	angular speed
t	time	Ω	vorticity

1. INTRODUCTION

Vertical axis wind turbine (VAWT) has the advantages of low cost, acceptable inflow wind in any direction and low noise (Li *et al.* 2013; Arpino *et al.* 2018). It is widely used in the suburban, urban environments and home applications. (Posa 2020a). When the wind turbine is in the wake of the upstream turbine, the inflow wind speed of the downstream wind turbine will decrease, and the turbulence intensity will increase (Wilson *et al.* 2018). Therefore, the research on the wake of the VAWT attracts attention.

In general, the flow field characteristic of the VAWT is governed by a broad range of factors, including blade geometry, tip speed ratio, solidity, blade number, rotor aspect ratio and Reynolds number. Hohman *et al.* (2020) studied the wake characteristics of VAWT using high resolution particle image velocimetry. The results showed that the wake momentum deficit of the VAWT is decreased with increasing sweep angle of the blade when the solidity of the rotor is constant. Almohammadi *et al.* (2014) investigated the effect of trailing edge shape on the VAWT. They found that the shape of blade trailing edge has an impact on the performance of VAWT, which should be accounted for in the design process. The solidity of the VAWT is related to the number of the blades. The numerical results indicated that the streamwise momentum deficit in the near wake of VAWT increases under the condition of high solidity. Due to the instability of the shear layers at the edge of the wake, an increase in tip speed ratio results in a higher momentum deficit in the wake of VAWT, but also a faster wake recovery (Posa 2020b). Maeda *et al.* (2017) investigated the effect of rotor solidity and aspect ratio on the power performance by panel method. The simulation results approved that the peak of power coefficient increases with the increase of the ratio of the rotor diameter and blade span length at the fixed solidity. Rezaeiha *et al.* (2018) further researched the effect of operational parameters on the performance of VAWT based on high-fidelity computational fluid dynamics method. They found that the operational parameters such as Reynolds number, tip speed ratio, and turbulence intensity have impact on the aerodynamic performance of VAWT.

Self-similarity is a common characteristic in shear flow. Satisfying self-similarity means that the variable in the wake flow reaches a stable state in the fully developed region, and the shape of its curve does not change with the downstream position (Ghosal 1997a). Individual scholars have studied the self-similarity characteristics of the wake of the horizontal axis wind turbine (HAWT) (Kabardin *et al.* 2017; Xiong *et al.* 2020). Lyu *et al.* (2019) performed numerical simulation focusing on the wake characteristics of HAWT. The results of large eddy simulation showed that the dimensionless mean velocity and Reynolds

stress curves in the wake of HAWT show self-similarity through an appropriate choice of characteristic scales of velocity and length. In recent years, numerous efforts have been spent on the wake characteristics and the establishment of wake models for HAWTs (Noura *et al.* 2016; Belkheir *et al.* 2012; Dahmouni *et al.* 2017; Kabir *et al.* 2019; Qian *et al.* 2022). However, the research on the wake characteristics of VAWT is not as extensive as that of HAWTs (Paraschivoiu 2002). For this reason, there are relatively few studies on the wake of the VAWT, especially in the variation of the wake characteristic parameters.

2. METHODOLOGY

2.1 Governing Equation

This study is based on the solution of the Navier-Stokes equations for incompressible flows under isothermal conditions. The continuity equation and Reynolds time-averaged Navier-Stokes equation are as follows:

$$\frac{\partial \rho}{\partial t} + \nabla \cdot (\rho \mathbf{v}) = 0 \quad (1)$$

$$\frac{\partial \rho \mathbf{v}}{\partial t} + \nabla \cdot (\rho \mathbf{v} \otimes \mathbf{v}) = -\nabla p + \nabla \cdot \boldsymbol{\tau} + \rho \mathbf{f} \quad (2)$$

Here, ρ is the air density, t is the time, \mathbf{v} is the velocity vector, p is the pressure, $\boldsymbol{\tau}$ is the surface stress vector, and \mathbf{f} is the body force vector per unit mass.

2.2 Transport Equation of γ - Re_θ Transition Model

The Reynolds-Averaged simulation is used to solve the flow field of the VAWT. The turbulence model considering transition is obtained by adding the two-equation γ - Re_θ transition model to the two-equation k - ω SST turbulence model. The transport equation of the transition model is composed of the momentum-thickness Reynolds number (Re_θ) transport equation and the intermittent factor (γ) transport equation (Menter *et al.* 2006).

The transport equation of the intermittent factor γ is:

$$\frac{\partial(\rho\gamma)}{\partial t} + \frac{\partial(\rho U_j \gamma)}{\partial x_j} = P_{\gamma 1} - E_{\gamma 1} + P_{\gamma 2} - E_{\gamma 2} + \frac{\partial}{\partial x_j} \left[\left(\mu + \frac{\mu_t}{\sigma_\gamma} \right) \frac{\partial \gamma}{\partial x_j} \right] \quad (3)$$

Here, ρ is the air density, t is the time, U_j is the velocity component, μ is the molecular viscosity, μ_t is the eddy viscosity, and $P_{\gamma 1}$, $E_{\gamma 1}$, $P_{\gamma 2}$, and $E_{\gamma 2}$ are the transition source, which are defined as:

Table 1. Parameters of the geometric model

Parameter	Blade length	Rotor radius	Pitch angle	Chord length	Maximum thickness
Value	1.02	0.85	6	0.225	0.035
Unit	m	m	deg	m	m

$$P_{\gamma 1} = C_{a1} F_{\text{length}} \rho S [\gamma F_{\text{onset}}]^{C_{\gamma 3}} \quad (4)$$

$$E_{\gamma 1} = C_{e1} P_{\gamma 1} \gamma \quad (5)$$

$$P_{\gamma 2} = C_{a2} \rho \Omega \gamma F_{\text{turb}} \quad (6)$$

$$E_{\gamma 2} = C_{e2} P_{\gamma 2} \gamma \quad (7)$$

Here, S is the strain rate, F_{length} is the length function of the control transition zone, F_{onset} and F_{turb} are the transition control function, and Ω is vorticity. The values of the constants are: $C_{a1}=2$, $C_{e1}=1$, $C_{a2}=0.06$, $C_{e2}=50$, $C_{\gamma 3}=0.5$, and $\sigma_{\gamma}=1.0$.

The transport equation of the momentum-thickness Reynolds number ($Re_{\theta t}$) is:

$$\frac{\partial(\rho R \tilde{e}_{\theta t})}{\partial t} + \frac{\partial(\rho U_j R \tilde{e}_{\theta t})}{\partial x_j} = \quad (8)$$

$$P_{\theta t} + \frac{\partial}{\partial x_j} \left[\sigma_{\theta t} (\mu + \mu_t) \frac{\partial R \tilde{e}_{\theta t}}{\partial x_j} \right]$$

where the source term is given by:

$$P_{\theta t} = C_{\theta t} \frac{\rho}{t} (Re_{\theta t} - R \tilde{e}_{\theta t}) (1.0 - F_{\theta t}) \quad (9)$$

Here, $Re_{\theta t}$ is the Reynolds number of the initial momentum thickness of the transition, $F_{\theta t}$ is the mixing function of the control source term, U is the local velocity, and the values of the constants are: $C_{\theta t}=0.03$, and $\sigma_{\theta t}=2.0$.

The detailed introduction of transition model and the description of parameters are shown in (Menter *et al.* 2006).

2.3 Geometric Model and Computational Condition

A two-bladed H-type VAWT with symmetric NACA0015 airfoil is invested in this study. The geometric parameters of the VAWT, including blade length, rotor radius, pitch angle, chord length, maximum thickness, are shown in Table 1.

2.4 Computational Domain and Grid Topology

As shown in Fig. 1, the three-dimensional rectangular domain is designed for the simulation and it consists of two parts: the rotating domain containing two blades and stationary domain surrounding the rotating domain (Rezaeiha *et al.* 2017; Lam *et al.* 2016). The length, width, and height of the rectangular domain are 15D, 6D and 5.6D, respectively, where D is the diameter of the wind turbine rotor. The distance between the wind

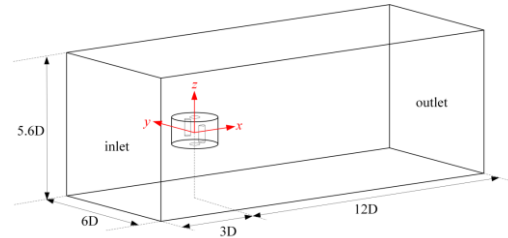


Fig. 1. Schematic of the computational domain and wind turbine location.

turbine and domain inlet is 3D. The arrangement of the coordinate system and the wind turbine is shown in Fig. 1.

The computational grid is made up of hexahedral cells everywhere. The O-grid is employed to create the grid around the blade. Mesh density may affect the simulation results. Thus, a mesh sensitivity is performed. According to the reference (Arpino *et al.* 2018), three different meshes are employed: 1) coarse mesh, composed by 5343565 cells; 2) medium mesh, composed by 11066268 cells; 3) fine mesh, composed by 14541298 cells. Fig. 2 shows the variations of the thrust coefficient during one revolution of the VAWT as a function of the azimuth angle for a tip speed ratio of 2.29. In order to ensure simulation results independence from grid and yet avoid prohibitive computational cost, simulations are carried out using medium mesh.

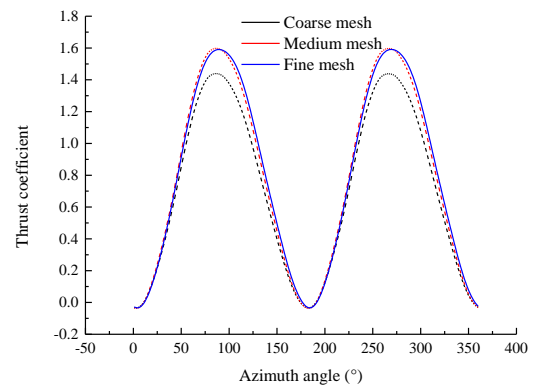
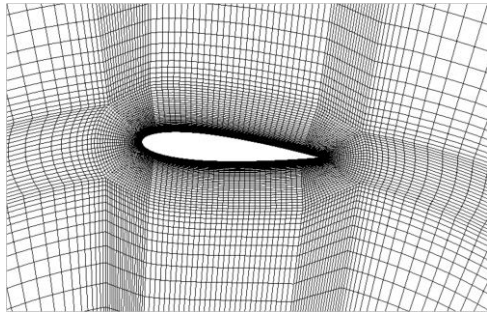


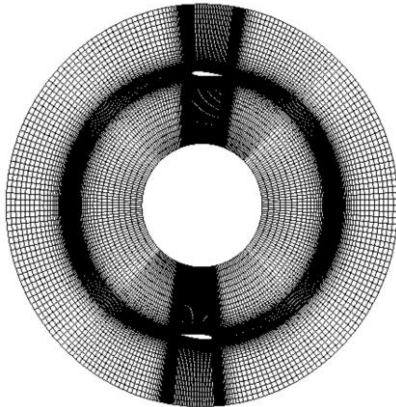
Fig. 2. Variations of the thrust coefficient during one revolution of the VAWT as a function of the azimuth angle for a tip speed ratio of 2.29.

As shown in Fig. 3 (a), 90 nodes are arranged in the chord direction of the blade, and encryption is performed at the leading edge and trailing edge. In order to adapt to the grid requirements of the turbulence model, the first grid spacing is about 0.04mm to ensure the most y^+ of the near wall less

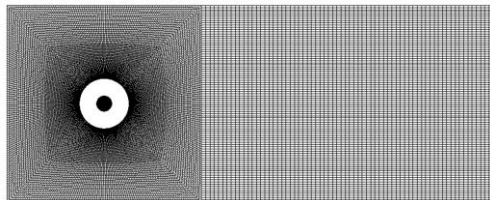
than 1, and geometric expansion ratio of 1.05 is employed. The maximum aspect ratio in the grid is 1450 and the minimum orthogonal quality is 0.21. The grids of the rotating domain and the stationary domain are shown in Fig. 3 (b) and Fig. 3 (c), respectively. Refined grids are produced in the wake regions to accurately capture the wake characteristics of the VAWT.



(a) Boundary layer grid around the blade



(b) Top view of the grid in the rotating domain



(c) Top view of the grid in the stationary domain
Fig. 3. Grid topology of the numerical model.

2.5 Boundary Condition and Solver Settings

The boundary conditions at the inlet, outlet, and other surface of the stationary domain are uniform velocity, zero surface averaged gauge pressure, and no-slip wall, respectively. The blade surface is the no-slip wall boundary condition. The interface between the stationary domain and rotating domain is set to the interface boundary condition. Furthermore, the inflow wind for the inlet is set at a speed (U_∞) of 7m/s under three calculation conditions. The rotor of the VAWT rotated counterclockwise (viewed from top to bottom) with an angular speed (ω) of 15.28 rad/s, 18.84 rad/s and 20.51 rad/s, respectively. In this study, the inflow wind speed and rotational speed of the rotor are

typically expressed in non-dimensional form by the tip speed ratio (λ), which is defined as $\lambda = \omega R / U_\infty$, where R is the radius of the rotor. Thus, the operating tip speed ratio (λ) of the wind turbine is 1.85, 2.29 and 2.52, respectively.

To take into account the unsteady effects, the numerical simulations were performed in transient condition. The SIMPLE algorithm is employed for the coupling of pressure and velocity. The 2nd order discretization is adopted both in time and space. The $k-\omega$ SST turbulence model considering transition shown in section 2 is used to model the turbulence. In the process of simulation, when the monitored physical quantity of the flow field changes periodically, it is considered that the flow field reaches the state of convergence.

3. VERIFICATION OF NUMERICAL CALCULATION METHOD

For convenience of description, Fig. 4 shows the schematic of the relationship between azimuth angle θ and blade position. The azimuth angle of 0° is located at the 12 o'clock position, and the rotor of the VAWT rotated counterclockwise (viewed from top to bottom). In order to verify the numerical method in section 2, the surface pressure and single blade torque coefficient of spanwise middle position at the typical azimuth ($0^\circ, 90^\circ, 180^\circ, 270^\circ$) are obtained by the numerical method, and the results are compared with the experimental results in (Li *et al.* 2016). As shown in Fig. 5, the abscissa is the non-dimensional chordwise position x/c (c is the chord length of the blade) and the ordinate is the pressure coefficient C_p of the blade for the optimum tip speed ratio of 2.29, where the pressure coefficient is defined as follow:

$$C_p = \frac{P}{0.5\rho U_\infty^2} \quad (10)$$

Here, P is the pressure of the blade surface and the position of the pressure measurement is at the rotor-equatorial plane, ρ is the air density and U_∞ is the inflow wind velocity.

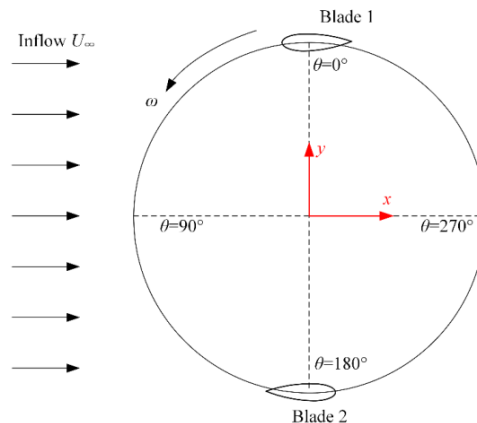


Fig. 4. Schematic of the relationship between azimuth angle θ and blade position.

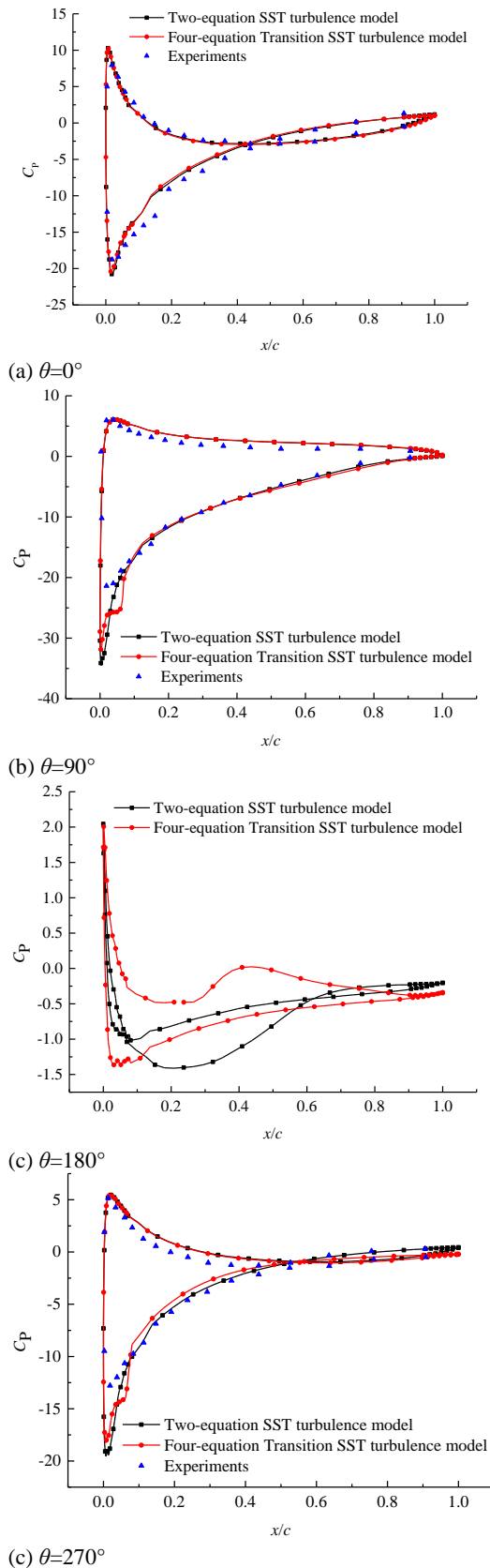


Fig. 5. Pressure coefficient distribution of the blade at the typical azimuth.

Since the experimental results of the surface pressure at 180° azimuth are difficult to obtain from

the reference, only the numerical results at 180° azimuth are given. The results from the Fig. 5 show that, the results obtained by the two-equation SST turbulence model are similar to those obtained by the four-equation transition SST turbulence model at most positions, but the results obtained by the four-equation transition SST turbulence model are closer to the experimental results in reference (Li *et al.* 2016) at the leading edge of the suction surface. Fig. 6 shows the comparison of the single blade torque coefficient of spanwise middle position with experimental results and CFD calculation at the typical azimuth. The comparison results are similar to those in reference (Li *et al.* 2016).

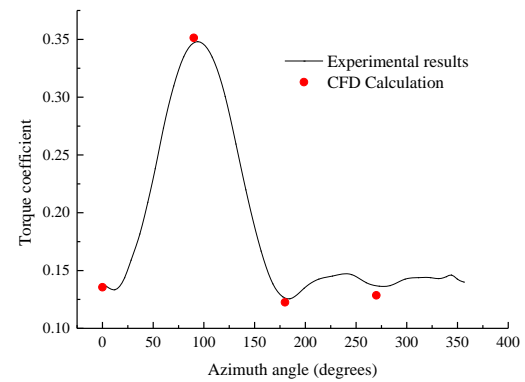


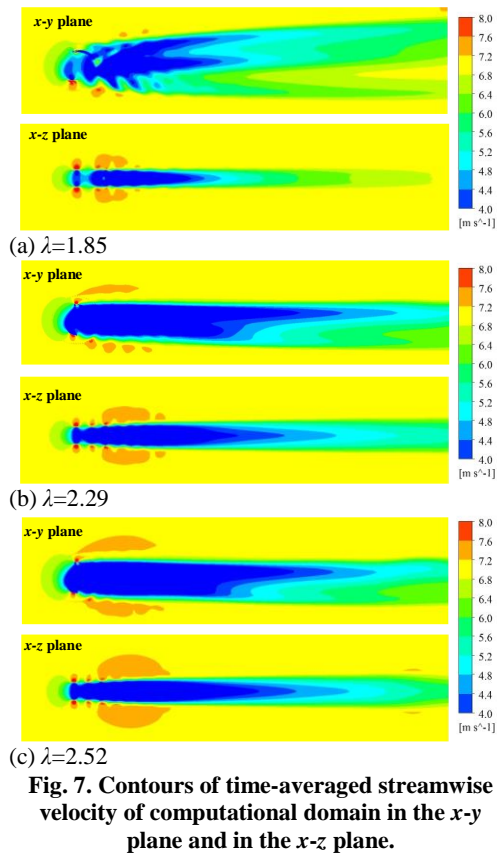
Fig. 6. Comparison of the single blade torque coefficient of spanwise middle position with experimental results and CFD calculation at the typical azimuth.

The above comparison results show that the numerical method used in this paper can predict the distribution of blade surface pressure and torque. The wake characteristics of the wind turbine are closely related to the momentum change of the flow direction (Mo *et al.* 2013). Therefore, accurate prediction of blade surface pressure can provide the necessary basis for subsequent wake analysis. In summary, the numerical method used in this paper can be used to study the wake characteristics of the wind turbine.

4. RESULTS

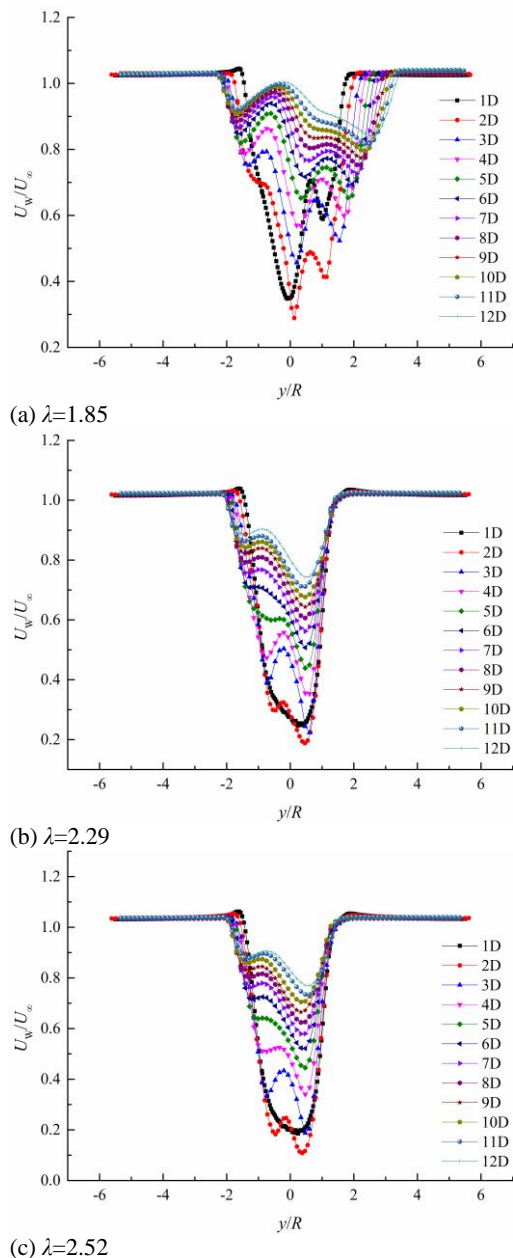
4.1 Streamwise Velocity Distribution in Wake Region

When the inflow wind passes through the rotor of the VAWT, the velocity in most of the wake region will decrease. In order to study the wake characteristics of the VAWT with different tip speed ratios, the time-average streamwise velocity of the computational domain in the x - y plane and x - z plane is obtained at 0° azimuth, and its contour is shown in Fig. 7. It can be seen from the figure that there is a clear boundary between the free flow region and the wake region of the VAWT, that is, there is a large velocity gradient between the two regions. At the edge of the near wake region, the shedding of the tip vortex can be clearly observed. As the distance to the downstream increases, the tip



vortex gradually dissipates and causes the wake area to expand. Furthermore, the smaller the tip speed ratio is, the faster the tip vortex dissipation speed, and the more obvious the expansion effect in the wake region.

In order to study the characteristics of the wake deficit under different tip speed ratios, the normalized velocity U_w/U_∞ is defined, where U_w is the streamwise velocity in wake region and U_∞ is the inflow wind velocity. The profiles of the mean streamwise velocity are investigated from 1D to 12D downstream distances of the rotor, where D represents the diameter of the wind turbine. Fig. 8 and Fig. 9 show the profiles of the time and space-averaged velocity U_w/U_∞ under different tip speed ratios in the x - y plane and x - z plane, respectively. As can be seen from Fig. 8 and Fig. 9, since the rotor of the wind turbine absorbs most of the energy in the wind, the velocity in most wake region decreases, that is, the dimensionless velocity U_w/U_∞ is less than 1. However, in the wake edge region, the velocity increases due to the shedding of blade tip vortex, that is, the dimensionless velocity U_w/U_∞ is greater than 1. This phenomenon can also be seen in Fig. 7. It can be seen from the Fig. 8 that the non-dimensional streamwise velocity of the wake region is obviously asymmetry in the x - y plane, that is, the location of maximum velocity deficit is not at the centerline of the wind turbine rotor. In the region on the left side of the x - y plane (viewed from front to back), due to the wind turbine rotor rotates counterclockwise (viewed from top to bottom), the rotation direction of the blade is opposite to the



velocity direction of the inflow wind velocity, and their interaction produces stronger inducing force for fluid, resulting in the streamwise velocity deficit on the left is significantly greater than on the right. Distribution of vorticity fields and streamlines around the rotor and near wake is shown in Fig. 10. In the x - z plane (left panel), vortex structures are shed into the near wake region due to downwind stall at $\lambda=1.85$. At $\lambda=2.29$ and $\lambda=2.52$, the stall effect is weakened and result in the decrease of the influence of vortex structure on near wake. Therefore, the streamwise velocity at position 1D in Fig. 8 is different from that at other positions, and the larger the tip speed ratio, the smaller the difference.

As shown in Fig. 9, the profiles of the mean streamwise velocity in the x - z plane is basically symmetrical. This phenomenon can be explained by the results of the x - z plane in Fig. 10 (right panel). It can be seen from Fig. 10 that vortex structures are distributed symmetrically in the wake region at any tip speed ratio. At $\lambda=1.85$, the distribution of vortex structures is different from other conditions, resulting in different velocity distribution in the near wake region. It can also be seen from the comparison that as the tip speed ratio increases, the wake deficit gradually increases.

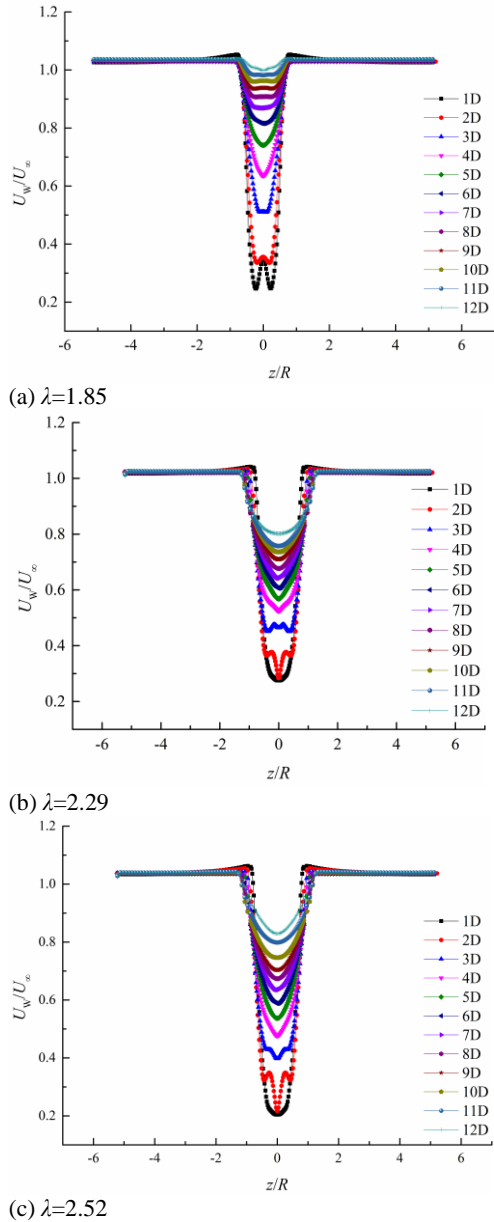


Fig. 9. Profiles of the mean streamwise velocity in the x - z plane at twelve downstream distances under different tip speed ratios.

Further studies show that the shape of the mean streamwise velocity in the far wake region is close to the same (see Fig. 9). In order to study the self-

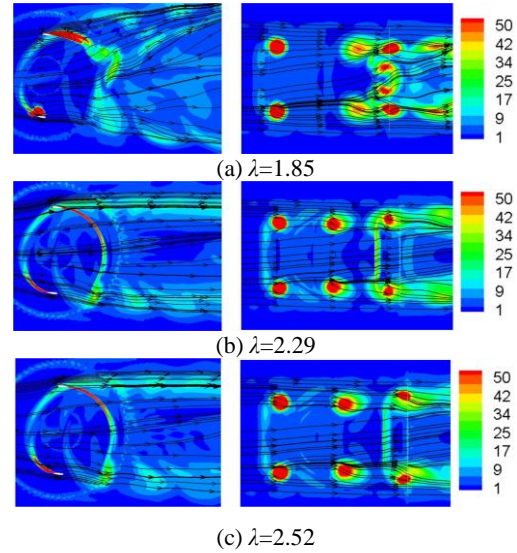


Fig. 10. Distribution of vorticity fields and streamlines around the rotor and near wake in the x - y plane (left) and in the x - z plane (right).

similarity characteristics of the streamwise velocity deficit in the x - z plane, the flow structure diagram and coordinate system position are defined in Fig. 11.

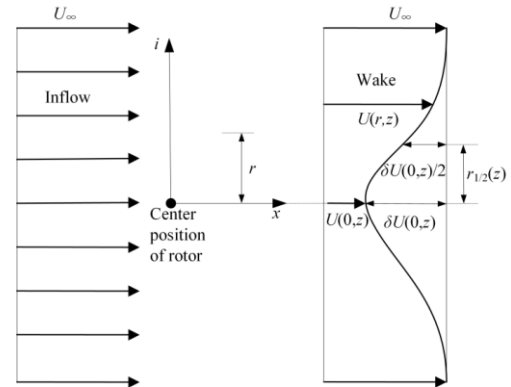


Fig. 11. Schematic diagram of the flow field structure and coordinate system position.

4.2 Self-similarity Characteristics of the Streamwise Velocity Deficit

The non-dimensional shape function of the streamwise velocity deficit is defined as follows:

$$f(\xi) = \frac{\delta U}{\delta U_{\max}} \quad (11)$$

Here, $\delta U = U_{\infty} - U_w$ is the streamwise velocity deficit, and δU_{\max} is the maximum streamwise velocity deficit.

In the x - z plane, the independent variable of the shape function is defined as follow:

$$\xi = \frac{r(z)}{r_{1/2}(z)} \quad (12)$$

Here, $r(z)$ is the radial distance from the wake center (location of maximum streamwise velocity deficit), and $r_{1/2}(z)$ is the half width of the wake, which is defined as:

$$U_w(r_{1/2}, z) = U_\infty - \frac{1}{2} \delta U_{\max} \quad (13)$$

Based on the assumption of uniform turbulent viscosity, the non-dimensional velocity deficit shape curve can be described as a Gaussian distribution function (Pope 2000):

$$f(\xi) = \exp(-\xi^2 \ln 2) \quad (14)$$

According to the above definition, Fig. 12 shows the comparison results of the non-dimensional streamwise velocity deficit curve and the Gaussian distribution curve at different downstream distances under different tip speed ratios. It can be seen that the shape of the non-dimensional streamwise velocity deficit in the far wake region is roughly similar, indicating that the streamwise velocity deficit satisfies the self-similarity from a certain downstream position. When $-1 \leq \xi \leq 1$, the non-dimensional streamwise velocity deficit curve basically coincides with the Gaussian distribution curve. At the edge of the wake region, the turbulent shear effect caused by tip vortex shedding is enhanced, and the difference between the non-dimensional streamwise velocity deficit curve and Gaussian distribution curve increase. Comparing the non-dimensional streamwise velocity deficit curves under different tip speed ratios, it can be seen that the greater the tip speed ratio is, the easier streamwise velocity deficit reach self-similarity state at downstream of the VAWT. This can be explained by the iso-surface plot of Q criterion shown in Fig. 13, that is, as the tip speed ratio increases, the wake dissipation speed increases.

5. CONCLUSION

In this paper, the wake deficit and self-similarity characteristics of a two-blade VAWT are studied under different tip speed ratios. The SST turbulence model with the addition of the γ - Re_θ transition model is performed to simulate the flow field characteristics. The rationality of the numerical calculation method is verified by comparing the numerical results and experimental results. The following conclusions are drawn from this study.

In the simulation of the VAWT, compared with the numerical results of the two-equation SST turbulence model, the results obtained by the four-equation transition SST turbulence model are more consistent with the experimental results.

The average streamwise velocity in the vertical plane of the VAWT wake region is symmetric, and the non-dimensional streamwise velocity deficit at different downstream positions remains self-similarity. Furthermore, the deficit curve basically coincides with the Gaussian distribution curve except for the edge of the wake region, and the greater the tip speed ratio is, the easier streamwise velocity deficit reach self-similarity state at downstream of wind turbine.

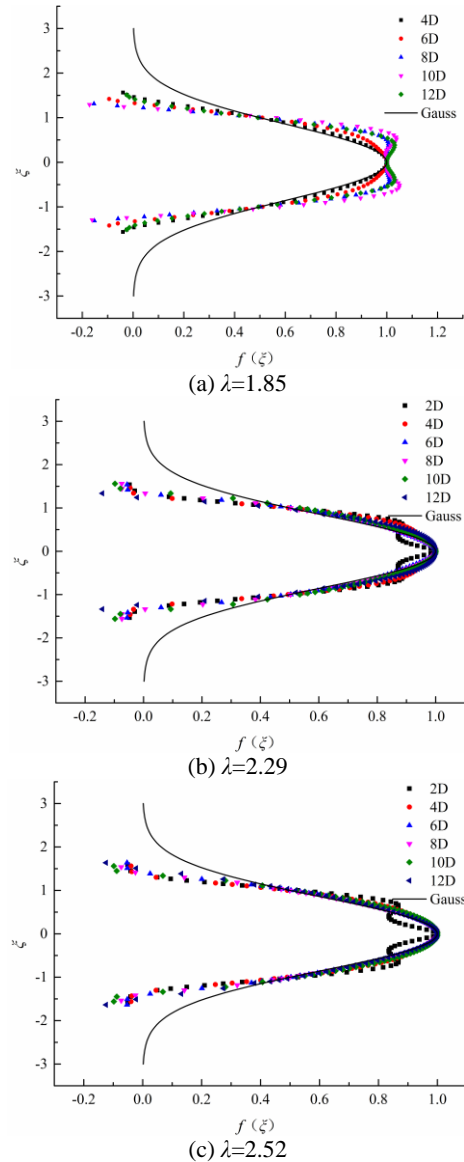


Fig. 12. Comparison of the non-dimensional streamwise velocity deficit curve and the Gaussian distribution curve at different downstream distances under different tip speed ratios.

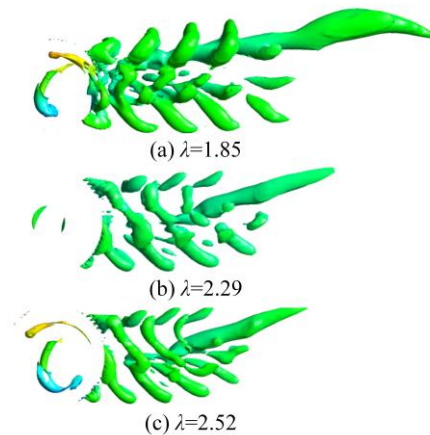


Fig. 13. Iso-surface plot of Q criterion under different tip speed ratios.

In the future study, the influence of other parameters, such as blade geometry, solidity, blade number, and rotor aspect ratio, on self-similarity characteristics of VAWT wakes will be studied. In addition, the self-similarity characteristics of the wake deficit will be used to establish the wake model of the VAWT.

ACKNOWLEDGEMENTS

This research was funded by the Young Scholars Science Foundation of Lanzhou Jiaotong University (Grant No. 2020017); Gansu Province Science Foundation for Youths (Grant No.20JR10RA264); Gansu University Innovation Fund Project (Grant No. 2021A-035); Tianyou Innovation Team Support Plan of Lanzhou Jiaotong University.

REFERENCES

- Almohammadi, K. M., D. B. Ingham, L. Ma and M. Pourkashanian (2014). 2-D-CFD analysis of the effect of trailing edge shape on the performance of a straight-blade vertical axis wind turbine. *IEEE Transactions on Sustainable Energy* 6(1), 228-235.
- Arpino, F., M. Scungio and G. Cortellessa (2018). Numerical performance assessment of an innovative Darrieus-style vertical axis wind turbine with auxiliary straight blades. *Energy Conversion and Management*, 171, 769-777.
- Belkheir, N., R. Dizene and S. Khelladi (2012). A numerical simulation of turbulence flow around a blade profile of HAWT rotor in moving pulse. *Journal of Applied Fluid Mechanics* 5(1), 1-9.
- Dahmouni, A. W., M. M. Oueslati and S. B. Nasrallah (2017). Experimental investigation of tip vortex meandering in the near wake of a horizontal-axis wind turbine. *Journal of Applied Fluid Mechanics* 10(6), 1679-1688.
- Ghosal, S. and M. M. Rogers (1997). A numerical study of self-similarity in a turbulent plane wake using large-eddy simulation. *Physics of Fluids* 9(6), 1729-1739.
- Hohman, T. C., L. Martinelli and A. J. Smits (2020). The effect of blade geometry on the structure of vertical axis wind turbine wakes. *Journal of Wind Engineering and Industrial Aerodynamics* 207, 104328.
- Kabardin, I. K., I. V. Naumov and V. L. Okulov (2017). An investigation of a self-similarity for local vorticity and velocity components in tip vortex cores of a rotor wake. *Journal of physics: Conference series* 899, 022008.
- Kabir, I. F. S. A. and E. Y. K. Ng (2019). Effect of different atmospheric boundary layers on the wake characteristics of NREL phase VI wind turbine. *Renewable energy* 130, 1185-1197.
- Lam, H. F. and H. Y. Peng (2016). Study of wake characteristics of a vertical axis wind turbine by two-and three-dimensional computational fluid dynamics simulations. *Renewable Energy* 90, 386-398.
- Li, C., S. Y. Zhu, Y. L. Xu, and Y. Q. Xiao (2013). 2.5D large eddy simulation of vertical axis wind turbine in consideration of high angle of attack flow. *Renewable Energy* 51, 317-330.
- Li, Q. A., T. Maeda, Y. Kamada, Murata, J., T. Kawabata, K. Shimizu, T. Ogasawara, A. Nakia and T. Kasuya (2016). Wind tunnel and numerical study of a straight-bladed vertical axis wind turbine in three-dimensional analysis (Part I: For predicting aerodynamic loads and performance). *Energy* 106, 443-452.
- Lyu, P., W. L. Chen, H. Li and L. Shen (2019). A numerical study on the development of self-similarity in a wind turbine wake using an improved pseudo-spectral large-eddy simulation solver. *Energies* 12(4), 643.
- Maeda, T., Y. Kamada, K. Shimizu, T. Ogasawara, A. Nakai and T. Kasuya (2017). Effect of rotor aspect ratio and solidity on a straight-bladed vertical axis wind turbine in three-dimensional analysis by the panel method. *Energy* 121, 1-9.
- Menter, F. R., R. B. Langtry, S. R. Likki, Y. B. Suzen, P. G. Huang and S. Völker (2006). A correlation-based transition model using local variables—part I: model formulation. *Journal of Turbomachinery* 128, 413-422.
- Mo, J. O., A. Choudhry, M. Arjomandi and Y. H. Lee (2013). Large eddy simulation of the wind turbine wake characteristics in the numerical wind tunnel model. *Journal of Wind Engineering and Industrial Aerodynamics* 112, 11-24.
- Noura, B., I. Dobrev, R. Kerfah, F. Massouh and S. Khelladi (2016). Investigation of the rotor wake of horizontal axis wind turbine under yawed condition. *Journal of Applied Fluid Mechanics* 9(6), 2695-2705.
- Paraschivoiu, I. (2002). *Wind turbine design: with emphasis on Darrieus concept*, 1st ed.; Polytechnic International Press: Montreal, Canada.
- Pope, S. B. (2000). *Turbulent flows*, 1st ed.; Cambridge: University Press: Cambridge, England, 96-168.
- Posa, A. (2020a). Dependence of the wake recovery downstream of a Vertical Axis Wind Turbine on its dynamic solidity. *Journal of Wind Engineering and Industrial Aerodynamics* 202, 104212.
- Posa, A. (2020b). Influence of tip speed ratio on wake features of a vertical axis wind turbine. *Journal of Wind Engineering and Industrial Aerodynamics* 197, 104076.
- Qian, G. W., Y. P. Song and T. Ishihara (2022). A control-oriented large eddy simulation of wind turbine wake considering effects of Coriolis

- force and time-varying wind conditions. *Energy* 239, 121876.
- Rezaeiha, A., H. Montazeri and B. Blocken (2018). Characterization of aerodynamic performance of vertical axis wind turbines: impact of operational parameters. *Energy Conversion and Management* 169, 45-77.
- Rezaeiha, A., I. Kalkman and B. Blocken (2017). CFD simulation of a vertical axis wind turbine operating at a moderate tip speed ratio: Guidelines for minimum domain size and azimuthal increment. *Renewable Energy* 107, 373-385.
- Wilson, D., S. Rodrigues, C. Segura, I. Loshchilov, F. Hutter, G. L. Buenfil, A. Kheiri, E. Keedwell, M. Ocampo-Pineda, E. Özcan, S. I. V. Peña, B. Goldman, S. B. Rionda, A. Hernández-Aguirre, K. Veeramachaneni and S. Cussat-Blanc (2018). Evolutionary computation for wind farm layout optimization. *Renewable Energy* 126, 681-691.
- Xiong, X. L., P. Lyu, W. L. Chen and H. Li (2020). Self-similarity in the wake of a semi-submersible offshore wind turbine considering the interaction with the wake of supporting platform. *Renewable Energy* 156, 328-341.